scientific reports

Check for updates

OPEN

Bridging the translational gap in radiotherapy: a human three-dimensional cell culture for evaluating neutron biological effects

Susanna Leva[1,2], Kazuyo Igawa[3]✉, Izumi Yamamoto[4], Yoshinori Sakurai[5], Natsuko Kondo[5], Kenji Izumi[6] & Kae Sato[7]

In radiation therapy, accurately estimating the relative biological effectiveness (RBE) is essential for the safe and effective clinical application of neutron radiation therapy. Current RBE evaluations primarily rely on two-dimensional (2D) colony formation assays. However, these models cannot fully capture tissue-level complexity and are not applicable to normal cells lacking colony-forming ability. This limits their clinical applicability. This study demonstrated that the dimensionality of the culture is a critical determinant of radiation sensitivity. While the biological effectiveness of neutron irradiation is systematically overestimated in conventional 2D monolayer systems, three-dimensional (3D) tissue-mimicking models more accurately reproduce the resistance of normal tissues observed in clinical settings. Specifically, we identified a dose-dependent thinning of the extracellular matrix at doses of 25 Gy or higher, suggesting that neutron-induced damage extends beyond cell death to include structural and microenvironmental damage. These findings offer direct insights into the estimation of clinical doses and the protection of normal tissues. While further refinement of model parameters, including cell density and microenvironmental composition, is necessary, the proposed 3D platform provides a clinically meaningful framework for evaluating radiation-induced toxicity in non-colony-forming normal tissues. By facilitating a more precise evaluation of radiation-induced tissue effects, this methodology has the potential to enhance the estimation of RBE and risk stratification, thus contributing to the development of more secure treatment protocols and the broader implementation of neutron therapy.

Neutron radiobiology represents a distinctive paradigm within radiation science, defined by the unique physical interactions of neutrons with biological matter and the complex patterns of energy deposition that ensue[1,2]. Unlike photons or charged particles, which predominantly interact with atomic electrons, neutrons are indirectly ionizing and deposit energy through nuclear interactions, generating cascades of high-linear energy transfer (LET) secondary particles[3]. These processes give rise to densely clustered DNA damage, challenging canonical models of radiation response and repair.

The biological consequences of neutron exposure span multiple domains, from space radiation biology, where secondary neutrons contribute substantially to astronaut risk[4], to radiation protection in high-energy physics environments[5–7]. In oncology, these unique properties are harnessed therapeutically in boron neutron

[1]Radiobiology Unit, Research and Development Department, CNAO National Center for Oncological Hadrontherapy, 27100 Pavia, Italy. [2]School for Advanced Studies (IUSS), Hadron Academy PhD Course, 27100 Pavia, Italy. [3]Institute for Emerging Medical Innovation, Okayama University, Okayama 700-8558, Japan. [4]Department of Oral and Maxillofacial Surgery, Graduate School of Medicine, Dentistry and Pharmaceutical Sciences, Okayama University, Okayama 700-8558, Japan. [5]Particle Radiation Oncology Center, Institute for Integrated Radiation and Nuclear Science, Kyoto University, Osaka 590-0494, Japan. [6]Division of Biomimetics, Faculty of Dentistry & Graduate School of Medical and Dental Sciences, Niigata University, Niigata 951-8514, Japan. [7]Department of Chemical and Biological Sciences, Faculty of Science, Japan Women's University, Tokyo 112-8681, Japan. ✉email: Igawakazuyo@okayama-u.ac.jp

capture therapy (BNCT), a modality that exploits neutron capture reactions to achieve highly localized, cell-selective cytotoxicity[2,8].

However, a fundamental yet underappreciated aspect of neutron radiobiology is the intrinsic biological activity of thermal neutrons in native tissue environments, independent of exogenous boron delivery[3]. Thermal neutrons, despite their low kinetic energy (~0.025 eV), induce biologically significant effects through nuclear capture reactions with endogenous elements, particularly nitrogen and hydrogen. The $^{14}N(n,p)^{14}C$ reaction generates high-LET protons, whereas $^{1}H(n,\gamma)^{2}H$ produces low-LET gamma radiation, together shaping a composite radiation field within tissues[1,9].

This duality underscores a key conceptual challenge: the biological effectiveness of neutrons cannot be fully understood through conventional radiobiological frameworks that are largely derived from photon-based systems[2,10]. Instead, neutron-induced damage reflects a multi-scale phenomenon, encompassing not only direct DNA damage but also perturbations of tissue architecture and microenvironmental integrity[11,12]. Consequently, accurate estimation of relative biological effectiveness (RBE) remains a central and unresolved issue in both radiation protection[7] and clinical translation[3,12].

Historically, the quantification of RBE has been conducted using two-dimensional (2D) monolayer cultures and clonogenic survival assays. Despite the fact that these approaches have yielded foundational insights, they are intrinsically reductionist and fail to capture the spatial, structural, and biochemical complexity of living tissues[13]. Notably, these models fail to incorporate the significance of cell-to-cell interactions and the influence of the extracellular matrix (ECM) on radiosensitivity. Furthermore, they do not consider the oxygen, nutrient, and signalling molecule gradients that have been identified as critical regulators of radiosensitivity[14].

The limitations of 2D systems have catalysed a paradigm shift toward three-dimensional (3D) tissue models, including spheroids and scaffold-based constructs, which more faithfully recapitulate tissue organization and microenvironmental heterogeneity. These models reveal that radiosensitivity is not an intrinsic cellular property alone but is emergent from multicellular architecture and context-dependent signalling networks[15]. As such, 3D systems offer a more physiologically relevant framework for interrogating neutron-induced biological effects and refining RBE estimation.

Importantly, this transition from 2 to 3D models reframes neutron radiobiology as a systems-level problem, in which radiation effects must be understood across multiple spatial and temporal scales from molecular damage to tissue-level dysfunction[13–16]. Within this context, features such as extracellular matrix remodelling and microenvironmental disruption emerge as critical determinants of radiation response, extending beyond traditional endpoints based solely on clonogenic survival[14,17–19].

In this study, we address these conceptual and methodological gaps by systematically comparing the effects of thermal neutron irradiation in 2D and 3D culture systems. Using controlled neutron exposures at the Kyoto University Research Reactor (KUR), we investigate how culture dimensionality shapes radiosensitivity and biological response across clinically relevant dose ranges. Furthermore, we integrate quantitative validation strategies to ensure robust assessment within complex 3D architectures.

By bridging physical dosimetry with advanced tissue-mimetic modelling, this work contributes to the emerging framework of next-generation radiobiology, in which experimentally tractable yet physiologically relevant systems are leveraged to refine risk assessment and inform precision radiotherapy strategies.

Results

Evaluation of radiobiological response in 2D and 3D models of stromal and cancer cells

The evaluation of relative cell viability across a neutron dose range of 0 to 25.8 Gy revealed a consistent dose-dependent reduction in viability for all cell lines tested in 2D monolayers (Fig. 1a, b). In the 2D stromal cell cultures, human umbilical vein endothelial cells (HUVEC) cells exhibited lower cell viability rates compared to patient-derived normal oral fibroblasts (NOF) and patient-derived cancer-associated fibroblasts (CAF), with a statistically significant difference emerging at 2.5 Gy ($^{*}p < 0.05$) (Fig. 1a). Similarly, the 2D cancer cell cultures showed a steady decrease in cell viability as the neutron dose increased, with lowly metastatic human oral squamous cell carcinoma (HSC-4) demonstrating higher radio sensitivity compared to the human osteosarcoma cells (MG-63) and highly metastatic human oral squamous cell carcinoma (HSC-3) at 2.5 Gy ($^{**}p < 0.01$) (Fig. 1b). Complementary morphological characterization of 2D monolayers and detailed viability metrics, including live cell percentage and mean cell diameter, are provided (Supplementary Fig. 1, 2).

For stromal cells cultured in the 3D model, the decrease in viability was attenuated with increasing neutron dose compared with that observed in 2D culture (Fig. 1c, d**).** Within the 3D stromal environment, no significant differences in viability were observed among the cell lines (Fig. 1c). Similarly, no marked reduction in viability was detected in the 3D tumour model across the dose range examined (Fig. 1d). Despite this overall stability, significant differences were observed at lower doses, particularly at 2.5 Gy ($^{****}p < 0.0001$) and 5.3 Gy ($^{*}p < 0.05$), where HSC-4 exhibited higher viability than HSC-3 and MG-63.

Direct comparisons between 2 and 3D cultures at different neutron doses (2.5, 5.3, 13.2, and 25.8 Gy) revealed significant differences in cell viability for most cell lines (Fig. 1e–h). At 2.5 Gy, significantly higher cell viability was observed in the 3D models than in the corresponding 2D cultures for HSC-4 ($^{****}p < 0.0001$) and HUVEC ($^{**}p < 0.01$) (Fig. 1e). This increased resistance in the 3D environment was also evident at 5.3 Gy, where highly significant differences were observed for HSC-3 and HUVEC ($^{****}p < 0.0001$), while HSC-4 and MG-63 showed significant differences ($^{**}p < 0.01$) (Fig. 1f). At 13.2 Gy, significant differences between 2 and 3D cultures were observed in all cell lines except NOF and CAF, with HSC-3, HSC-4, HUVEC, and MG-63 showing the highest level of statistical significance ($^{****}p < 0.0001$) (Fig. 1g). At 25.8 Gy, significant differences between culture conditions remained evident. HSC-3 and HUVEC continued to show highly significant differences ($^{****}p < 0.0001$), whereas HSC-4 and MG-63 also maintained significantly higher viability in 3D culture ($^{**}p < 0.01$), despite the apparent plateau in the dose–response relationship at higher doses (Fig. 1h).

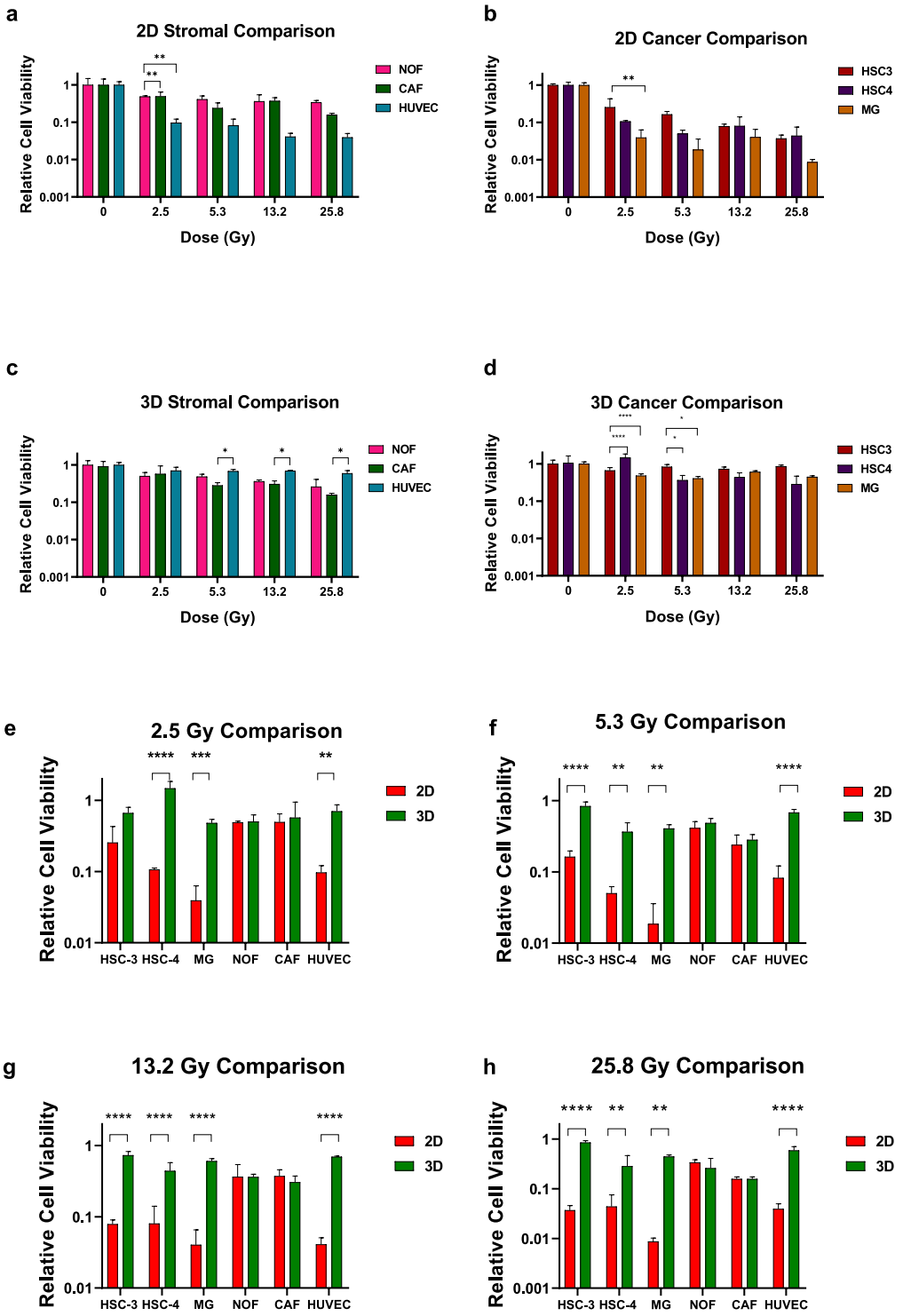

Fig. 1. Comparative radiobiological response of 2D and 3D cultures. **(a–b)** Survival fractions of stromal **(a)** and cancer **(b)** cell lines in 2D monocultures across a neutron dose range (0–25.8 Gy). **(c–d)** Survival fractions of stromal **(c)** and cancer **(d)** cell lines in 3D scaffolds. **(e–h)** Direct comparison between 2D (red bars) and 3D (green bars) survival fractions at 2.5 Gy **(e)**, 5.3 Gy **(f)**, 13.2 Gy **(g)**, and 25.8 Gy **(h)**. All values are shown on a semi-logarithmic scale and represent the mean ± standard deviation (SD). Statistical analysis for panels **(a–d)** was performed using Two-way ANOVA followed by Tukey's multiple comparisons post-hoc test. Statistical analysis for panels (e–h) was performed using Two-way ANOVA followed by Sidak's multiple comparisons post-hoc test. *$p < 0.05$, **$p < 0.01$, ***$p < 0.001$, ****$p < 0.0001$.

In contrast, the NOF and CAF lines demonstrated a remarkably stable response regardless of the culture system. Across the entire neutron dose range, no significant differences were observed between the 2D and 3D configurations for these two patient delivered cells (Fig. 1 **e, h**). Both NOF and CAF consistently exhibited an intrinsic radio resistance, with a low reduction in viability that remained independent of the culture model.

Non-linear regression curve fitting and quantitative assessment of IC_{50} and RBE estimation

The non-linear regression analysis of relative cell viability data revealed distinct dose–response fitting profiles depending on both the radiation type and the culture dimensionality across all examined cell lines (Fig. 2). In the conventional 2D monolayer configurations, the fitting curves for both X-rays and neutrons exhibited a classic sigmoidal dose-dependent decrease. For most cell lines, including HSC-3, HSC-4, and NOF, the neutron fitting curves showed a marked leftward shift compared to their respective X-ray counterparts, reflecting an enhanced reduction in cell viability at lower dose levels (Fig. 2a, b, d).

Conversely, the 3D scaffold configurations demonstrated highly altered fitting profiles characterized by a distinct lack of sigmoidal descent. For several cell populations, including HSC-3, NOF, and HUVEC under neutron irradiation, as well as HSC-4, MG-63, NOF, CAF, and HUVEC exposed to X-rays, the viability curves stalled at high plateaus or remained remarkably flat across the entire experimental dose range, failing to converge toward a standard descending sigmoidal model (Fig. 2). A notable exception was observed for the MG-63 line, which exhibited an immediate threshold collapse below the 50% viability mark at the lowest experimental dose of 2.5 Gy in both 2D and 3D configurations under neutron beams (Fig. 2c). From these mathematical regression profiles, IC_{50} values were extracted to estimate the final experimental RBE (Supplementary Table 1). As summarized in Supplementary Table 1, while the tightly fitted 2D configurations allowed a definitive calculation of RBE (yielding values of 4.7 for HSC-3 and 2.1 for NOF), the marked radioresistance observed in the 3D scaffolds rendered the IC_{50} parameters as Not Reached (N.R., > 25 Gy), consequently qualifying the final RBE as Not Computable (N.C.) for almost all 3D culture condition.

Histological assessment of 3D scaffolds in cancer and stromal cell models

The structural impact of neutron irradiation on the 3D models was evaluated by integrating qualitative histological observations with a quantitative approach to measure tissue parameters. As demonstrated in the representative sections of the 3D cancer scaffolds, there is a visible and progressive contraction of the scaffold matrix as the neutron dose increases from 0 to 25.8 Gy (Fig. 3a). For the stromal models (NOF, CAF, HUVEC), this structural response was confirmed by the quantitative analysis of scaffold thickness, where a dose-dependent thinning is recorded for all stromal lines (Fig. 3b). Parallel to the matrix contraction, the nuclear count analysis indicated that the total number of stromal cells within the 3D environment underwent a slight reduction in a dose dependent manner (Fig. 3c). A similar pattern was observed for the 3D cancer scaffold. The quantitative measurement of scaffold thickness showed a significant thinning across all cancer models (Fig. 3d), mirroring the morphological contraction seen in the histological samples (Fig. 3a). Finally, the relative total cell counts for the cancer models exhibited a decreasing trend as the neutron dose increased (Fig. 3e).

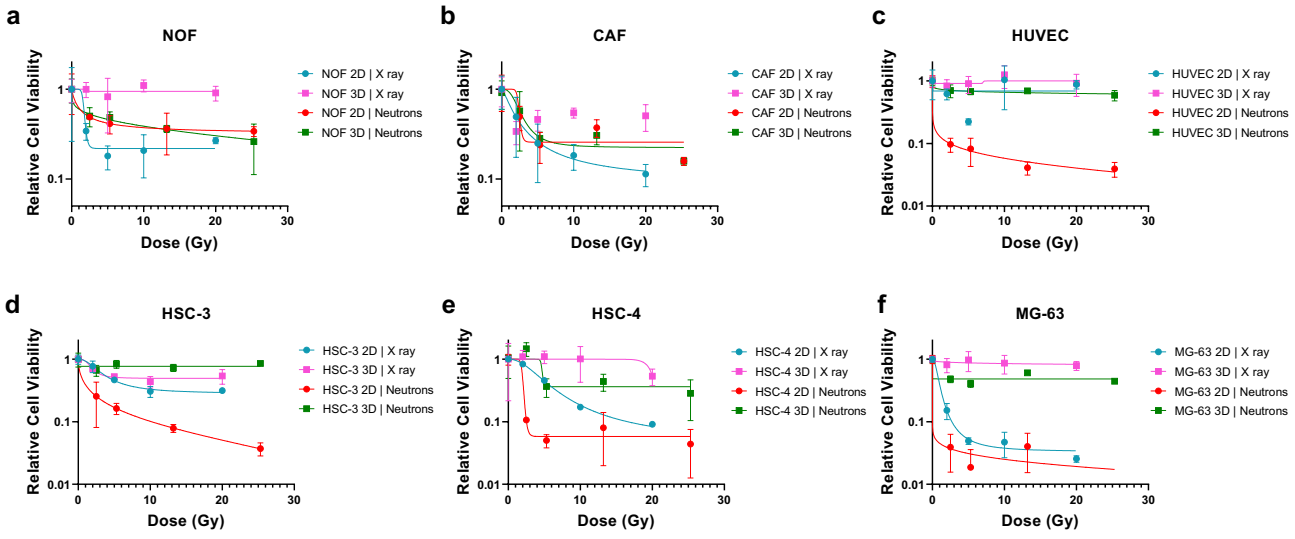

Fig. 2. Non-linear regression curve fitting for absolute IC_{50} estimation under X-ray and thermal neutron irradiation. Dose–response profiles mapping relative cell viability at 72 h post-irradiation across 2D monolayer configurations (light blue lines/circles for X-rays; red lines/circles for neutrons) and 3D scaffold-based architectures (pink lines/squares for X-rays; green lines/squares for neutrons) for: **(a)** HSC-3, **(b)** HSC-4, **(c)** MG-63, **(d)** NOF, **(e)** CAF, and **(f)** HUVEC. Data points represent the mean ± standard deviation (SD).

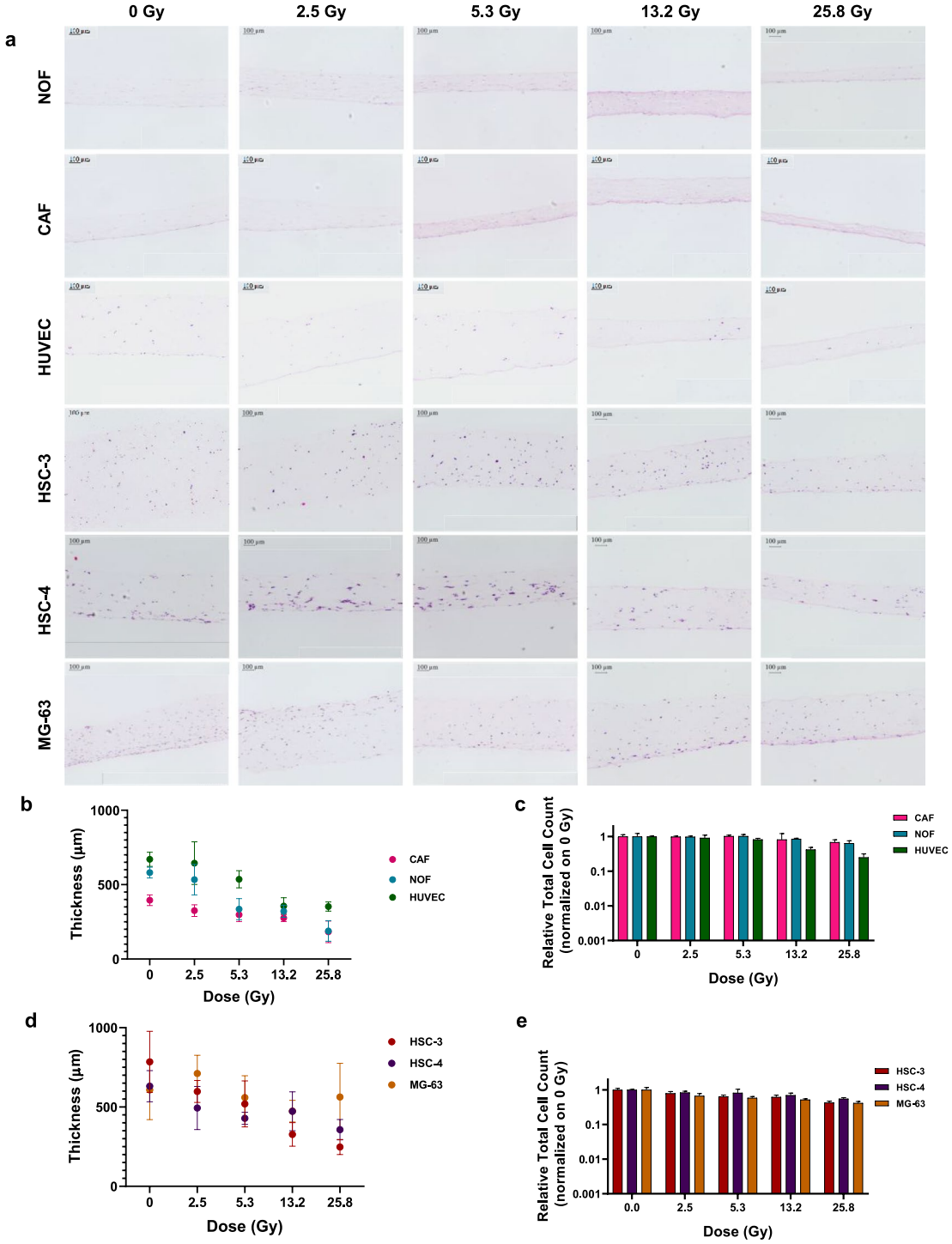

Fig. 3. H&E representative images and histological analysis of 3D constructs. **(a)** Representative histological sections of NOF, CAF, HUVEC, HSC-3, HSC-4 and MG-63 3D constructs stained with haematoxylin and eosin (H&E) at doses from 0 to 25.8 Gy (scale bar = 100 µm). **(b)** Quantitative analysis of NOF, CAF, and HUVEC constructs thickness (scale bar = 100 um) as a function of neutron dose. **(c)** Total nuclear count per section of NOF, CAF and HUVEC scaffolds derived from quantitative histological analysis, normalized to 0 Gy controls. **(d)** Quantitative analysis of HSC-3, HSC-4 and MG-63 constructs thickness (scale bar = 100 um) as a function of neutron dose. **(e)** Total nuclear count per section of HSC-3, HSC-4 and MG-63 scaffolds derived from quantitative histological analysis, normalized to 0 Gy controls. All data are shown as mean ± SD.

Comparative validation of cell counting methodologies in 3D scaffolds

Figure 4 illustrates the differences in cell counts obtained using three distinct methodologies across the tested cells lines. Dose–response analyses revealed that total cell numbers derived from histological assessment (red circles) and live cell counts following collagenase dissociation (blue circles) exhibited concordant and progressively decreasing trends with increasing radiation dose. This concordance was supported by positive Pearson correlation coefficients, most prominently in HUVEC (Fig. 4c; r = 0.69, P = 0.197) and MG-63 (Fig. 4f r = 0.86, P = 0.063). Although similar trends were observed in NOF and HSC-4, these did not reach statistical significance (r = 0.65 and r = 0.64, respectively). In contrast, total cell counts derived from enzymatic digestion (red circles) diverged substantially from the other two methodologies. A strong negative correlation was observed in NOF (Fig. 4a; r = −0.89, P = 0.041), indicating an inverse relationship between automated counts and histological measurements. Comparable inverse trends were identified in MG-63 (Fig. 3f; r = −0.64, P = 0.241) and 2–3 (Fig. 4d; r = −0.58, P = 0.310), whereas the correlation was negligible in CAF (Fig. 4b; r = −0.20, P = 0.743). The robustness of 3D cell quantification was further supported by the stability of live cell size distributions across the dose range (Supplementary Figs. 1**d, f and 2d, f**).

Discussion

RBE remains a central yet incompletely resolved parameter in radiobiology, governing the balance between therapeutic efficacy and normal tissue safety[1,7]. A major barrier to its accurate estimation lies in the continued reliance on clonogenic assays, which, despite their status as the conventional gold standard, are fundamentally unsuitable for primary normal cells[13,14,20]. Unlike immortalized cancer cell lines, primary fibroblasts and endothelial cells lack sufficient proliferative capacity to form discrete colonies, thereby precluding reliable RBE quantification using traditional methodologies[15,17].

This methodological constraint has broad implications. There is an urgent need for alternative models to reliably estimate RBE of healthy tissues, a factor of crucial importance for setting occupational exposure limits in nuclear facilities[5–7] and assessing risks for cosmic radiation exposure during space missions[4]. This methodological gap is equally critical in the clinical optimization of BNCT[12], where treatment protocols are primarily governed by the tolerance thresholds of healthy tissues rather than solely by the dose delivered to the tumor[21,22].

Our findings demonstrate that culture dimensionality fundamentally reshapes radiobiological responses. The 2D monolayer systems consistently overestimate neutron-induced cytotoxicity, as evidenced by steep dose response relationships across both normal and cancer cells (Fig. 1). This overestimation is quantitatively confirmed by our non-linear regression analysis, where tightly fitted 2D curves allowed the direct extraction of absolute IC_{50} values and computable experimental RBEs, yielding baseline values that reach up to 4.7 specifically for the responsive HSC-3 cancer cells, and 2.1 for NOF normal fibroblasts (Supplementary Table 1**).** For instance, the pronounced radiosensitivity of HUVEC in 2D, where viability decline to approximately 0.1 at doses as low as 2 Gy stands in clear contrast to clinical observations[23], in which vascular injury typically manifests at substantially higher dose levels (Fig. 1a). Similarly, the exaggerated sensitivity of cancer cells in 2D would imply that neutron irradiation alone is sufficient for tumour eradication, contradicting the established requirement for boron-mediated dose amplification in BNCT[24].

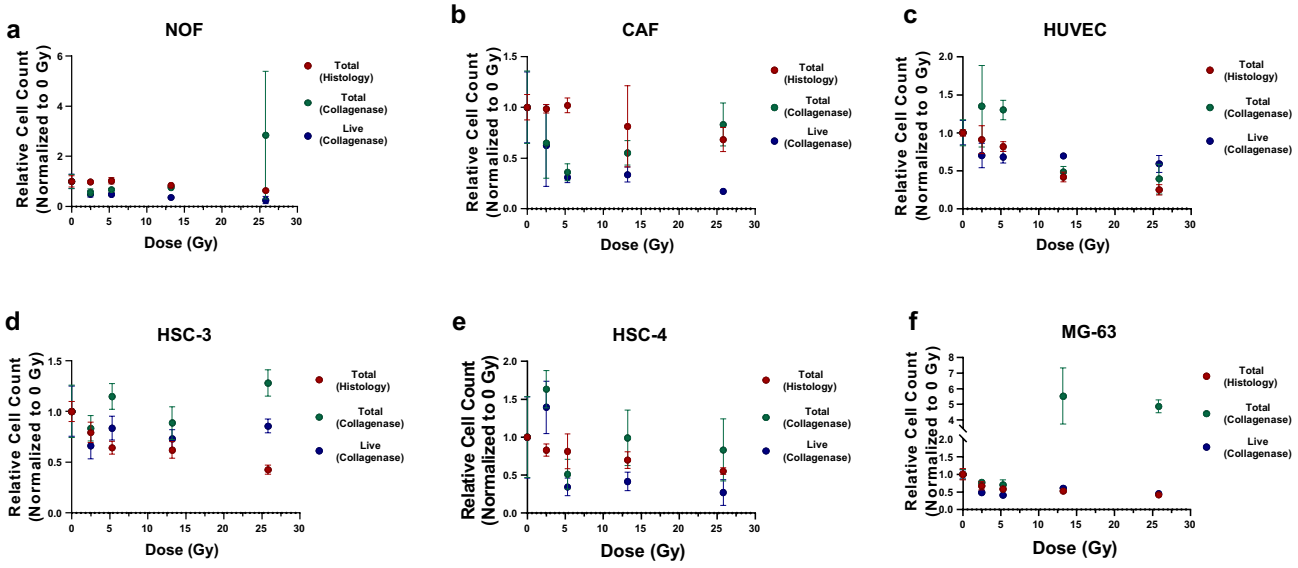

Fig. 4. Methodological evaluation for cell counting in 3D scaffolds. **(a-f)** Dose–response trends comparing Total Histology (red), Total Cell Count via Collagenase (green), and Live Cell Count via Collagenase (blue) for: **(a)** NOF, **(b)** CAF, **(c)** HUVEC, **(d)** HSC-3, **(e)** HSC-4, and **(f)** MG-632. All data are shown as mean ± SD normalized to respective 0 Gy. Statistical validation was performed using a Pearson correlation matrix for each cell line to assess inter-methodological consistency.

In contrast, 3D tissue-mimetic models provide a more physiologically relevant representation of radiation response (Fig. 1e-h, Fig. 2). Across all examined cell populations, relative viability remained above 0.1 even at doses up to 25 Gy, reflecting a degree of radioresistance that more closely aligns with clinical tolerance thresholds. As a direct consequence of this tissue-level resistance, the 50% viability threshold was frequently N.R., rendering the classical IC_{50} parameter and the subsequent RBE mathematically N.C. in the 3D configurations (Supplementary Table 1). Rather than an experimental limitation, this non-computability highlights a compelling biophysical hypothesis: the hydrogen-rich collagen hydrogel matrix could potentially act as a natural moderator. Within this tridimensional architecture, elastic scattering might attenuate the active neutron fluence, while thermal neutron capture reactions by hydrogen atoms $^{1}H(n,\gamma)^{2}H$ could partially shift the local radiation field properties toward lower-LET secondary gamma rays before reaching the embedded cells. Notably, patient-derived fibroblast populations (NOF and CAF) exhibited remarkable stability across both dimensional contexts, suggesting that stromal components may serve as intrinsic determinants of tissue resilience. The concordance between these experimental observations and the known clinical tolerance of oral mucosa in BNCT supports the validity of our model and underscores the capacity of 3D systems to recapitulate human tissue responses[22–26]. Moreover, the ability of patient-derived NOF models to reproduce clinically relevant dose response behaviour indicates that our experimental platform faithfully captures key features of human stromal biology. Consequently, the 3D scaffold-based environment provides a verisimilar framework for assessing the biological effectiveness of thermal neutrons[21,27].

Similarly, the greater resistance observed in the 3D models following X-ray irradiation may be attributable to microenvironmental factors rather than physical attenuation of the radiation beam (Fig. 2). The scaffold matrix may create localized hypoxic regions, thereby reducing the oxygen-dependent indirect DNA damage induced by photon irradiation. Furthermore, enhanced cell–cell and cell–matrix interactions within the three-dimensional microenvironment may activate signalling pathways associated with cell adhesion-mediated radioresistance. Together, these factors may contribute to the reduced radiation sensitivity observed in the 3D cultures.

Importantly, our findings extend beyond cell viability to encompass structural and microenvironmental responses[28,29]. Thermal neutron irradiation induced dose-dependent alterations in ECM integrity, evidenced by progressive scaffold thinning (Fig. 3). This phenomenon likely reflects localized energy deposition from nitrogen capture reactions, in which high-LET protons disrupt molecular bonds within collagen and polymer networks. These observations support a broader conceptualization of neutron-induced damage as a multi-scale process, integrating molecular, cellular, and tissue-level effects[28–30].

From a methodological perspective, the integration of complementary quantification strategies strengthens the robustness of our findings. By combining enzymatic dissociation-based viability analysis with automated histological image quantification, and validating consistency through Pearson correlation analysis, we establish a reproducible framework for analysing complex 3D systems (Fig. 3). This multi-modal approach mitigates the limitations inherent to each individual method and enhances confidence in the observed biological trends.

Although the current model is characterized by relatively low cellular density and a high matrix-to-cell ratio, these features highlight an important conceptual shift. Rather than prioritizing clonogenic expansion, 3D systems enable assessment of tissue-level integrity, which is particularly relevant for non-clonogenic cell populations such as fibroblasts and endothelial cells. In this context, the apparent limitation of reduced colony formation becomes a strength, allowing evaluation of radiation effects in a framework that more closely reflects in vivo tissue organization.

Taken together, our findings support a redefinition of neutron radiobiology as a systems-level discipline, in which biological effectiveness emerges from the interplay between cellular damage, tissue architecture, and microenvironmental dynamics. By demonstrating that 3D models provide a more accurate and clinically relevant platform for RBE estimation, this work contributes to the development of next-generation radiobiological frameworks that may ultimately inform safer and more precise neutron-based therapies.

Conclusions

Our study establishes three-dimensional tissue models as a clinically relevant platform for redefining RBE in neutron irradiation, addressing a critical gap in the assessment of normal tissue toxicity. By capturing multi-scale biological responses beyond clonogenic survival, this approach enables more accurate risk stratification and dose optimization. These advances provide a foundation for safer implementation and broader clinical adoption of neutron-based therapies, including BNCT.

Materials and methods

Cell lines and culture conditions

The following cell lines were employed: human oral squamous cell carcinoma (OSCC) lines HSC-3 (JCRB0623, JCRB) and HSC-4 (JCRB0624, JCRB), the human osteosarcoma line MG-63 (IFO50108 JCRB), and human umbilical vein endothelial cells (HUVEC). Additionally, patient-derived normal oral fibroblasts (NOF) and cancer-associated fibroblasts (CAF) were provided by Niigata University (Ethical Approval #2022–0300). NOF and CAF were isolated from cancer-negative and cancer-positive sites of the same patient, respectively, as previously described[17,21], and used between passages 1 and 4.

HUVEC were maintained in KBM medium (KBM VEC-1 Basal Medium, Kohjin Bio, cod. 16,030,110) according to the manufacturer's instructions. All other cell types were cultured in Alpha Modified Eagle Medium (α-MEM; Nacalai Tesque Inc., Kyoto, Japan) supplemented with 10% heat-inactivated fetal bovine serum (FBS; Corning, NY, USA) and 1% penicillin/streptomycin (10,000 U/mL and 10,000 μg/mL; Nacalai Tesque Inc.). All cultures were maintained in a humidified atmosphere at 37 °C with 5% CO_2.

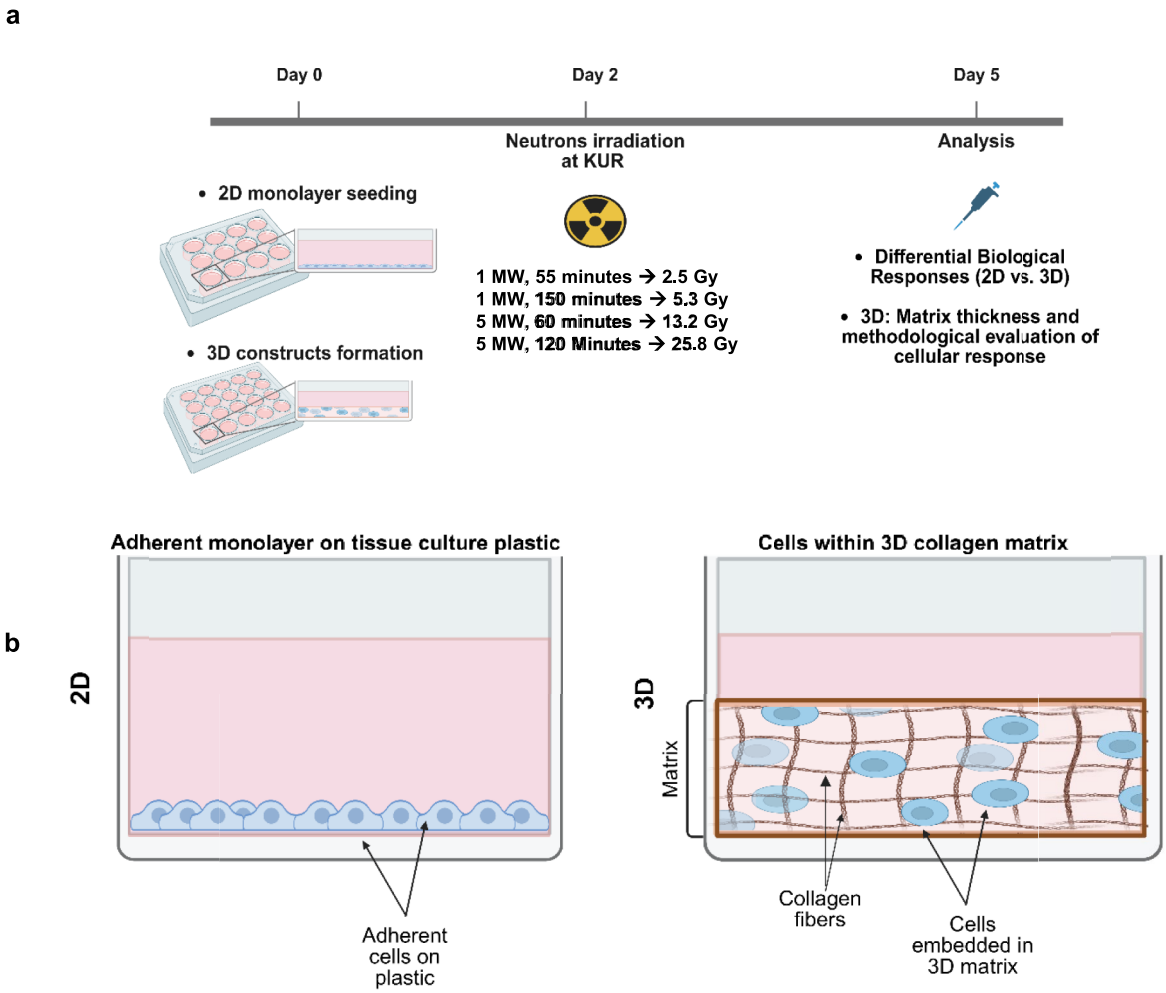

Fig. 5. Experimental set-up and workflow. **(a)**The schematic summarizes the sequential procedures from model establishment, irradiation and final aims. **(b)** Comparison of the culture dimensionality configurations: 2D model (left) and 3D model (right).

2D and 3D cell culture

For 2D experiments, cells were seeded at a density of 2×10^4 cells/well in 12-well plates (Thermo Fisher Scientific) with 2 mL of medium for well (Fig. 5a). After 48 h, prior to irradiation, the culture medium was aspirated from the plates. Following the exposure, the samples were immediately replaced with fresh culture medium.

For 3D models, a cold-prepared extracellular matrix was used, consisting of 7 parts of cell matrix (Nitta Gelatin, Japan), 2 parts 5 × DME (Nitta Gelatin, Japan), and 1 part of reconstruction buffer (Nitta Gelatin, Japan). All procedures were performed on ice to prevent premature polymerization. Cells were suspended in the matrix at a final concentration of 6×10^5 cells/mL. A 500 µL volume of the cell–matrix suspension was seeded into each well of a 24-well plate (Thermo Fisher Scientific) and incubated at 37 °C for 30 min to allow gelation (Fig. 5a). After polymerization, 1 mL of culture medium was added. After 48 h, prior to irradiation, the culture medium was aspirated from the plates. Following the exposure, the samples were immediately replaced with fresh culture medium.

Following neutron irradiation, both 2D monolayer cultures and 3D constructs were maintained in humified atmosphere at 37 °C with 5% CO_2 for a period of 72 h prior to further experimental procedures (Fig. 5b). The 72 h post-irradiation time point (corresponding to Day 5 of the overall protocol) was chosen as the optimal experimental window for the cell viability assay. This timeframe allows sufficient time for radiation-induced cell death to fully manifest, ensuring that damaged cells undergo membrane rupture and can be accurately quantified by the trypan blue exclusion test. Furthermore, evaluating cell viability at 72 h prevents the confounding effects of cellular overgrowth and nutrient depletion in the untreated (0 Gy) control groups, which would occur at longer incubation periods, thereby ensuring a reliable baseline for comparison.

Irradiation protocol

Neutron irradiation was performed at the Kyoto University Research Reactor (KUR). Both 2D monolayers and 3D constructs were exposed to reactor power levels of either 1 MW or 5 MW to achieve the target absorbed doses (Fig. 5a). Specifically, doses of 2.5 ± 0.5 Gy and 5.3 ± 0.5 Gy were delivered at 1 MW with exposure times of 55 and 150 min, respectively. Higher doses of 13.2 ± 1.5 Gy and 25.8 ± 1.9 Gy were obtained by operating the reactor at 5 MW for 60 and 120 min, respectively. To verify the accuracy of the delivered neutron fluence, gold foil dosimeters and thermoluminescent dosimeters (TLD) were placed directly on the culture plates during irradiation[19].

Reference X-ray irradiation was performed on Day 2 of the experiment for both 2D monolayer cultures and 3D scaffold models. Irradiation was carried out using a compact benchtop X-ray system (MX-80Labo; mediXtec Corporation, Chiba, Japan) operated at 80 kV and 1.25 mA. Samples were positioned at a fixed source-to-sample distance, with the cell layer or upper surface of the 3D construct facing the X-ray source. Prior to irradiation, the culture medium was temporarily removed, and the plates were placed in the irradiation chamber. Cells were exposed to single doses of 0, 2, 5, 10, or 20 Gy. After irradiation, fresh culture medium was added, and the samples were returned to standard culture conditions until subsequent analysis.

Viability analysis

2D cultures cells were detached using 0.025% trypsin/EDTA (NACALAI TESQUE Inc., Kyoto, Japan) and counted via trypan blue exclusion (Invitrogen, USA). The matrix of 3D scaffold was digested using a collagenase solution (0.1 g of collagenase and 14.7 mg of $CaCl_2$ in 50 mL H_2O) at 37 °C under gentle agitation for 60 min. Following centrifugation and resuspension cells were counted via trypan blue exclusion (1:1 dilution). Total cell numbers, live cell numbers and mean diameter were assessed using an automated cell counting system (Countess II FL, Invitrogen, USA).

Histology analysis

3D cell culture models were fixed in 4% paraformaldehyde (PFA), embedded in paraffin, and sectioned at 5 µm. Sections were stained with Hematoxylin and Eosin (H&E) and imaged using an all-in-one fluorescence microscope (BZ-X800, Keyence, Osaka, Japan).

Quantitative analysis was conducted using ImageJ Fiji (version 1.54f.; National Institutes of Health, Bethesda, MD, USA). Regions of interest (ROIs) were manually defined, and tissue segmentation was performed via grayscale thresholding to generate binary masks. Total tissue area, nuclei count (via particle analysis), and apparent tissue thickness (vertical height of the bounding box) were calculated from calibrated images.

Statistical analysis

All experimental procedures were performed using three to four independent samples per condition. Statistical evaluations were performed using GraphPad Prism 8 (GraphPad Software, San Diego, CA, USA). Data are expressed as mean ± standard deviation (SD) and, where applicable, normalized to the corresponding 0 Gy control. To evaluate the effects of radiation dose, cell line, and culture system (2D vs. 3D), two-way analysis of variance (ANOVA) was employed. Multiple comparisons were conducted using Tukey's post-hoc test to assess differences among multiple groups, while Sidak's post-hoc test was used for comparisons between specific conditions (e.g., 2D vs. 3D).

To estimate IC_{50} values, relative cell viability was plotted against radiation dose using GraphPad Prism software (GraphPad Software, San Diego, CA, USA), and dose–response curves were generated by nonlinear regression analysis. The IC_{50} was defined as the radiation dose required to reduce cell viability by 50% relative to the untreated control group. RBE was calculated as the ratio of the IC_{50} value obtained following X-ray irradiation to that obtained following neutron irradiation.

For histological and counting data where single factors were analysed, one-way ANOVA was applied. The consistency between different cell counting methodologies was evaluated using the Pearson correlation coefficient (r).

Statistical significance was defined as $P < 0.05$, with levels indicated as $^{*}p < 0{,}05$, $^{**}p < 0.001$, $^{***}p < 0.001$ and $^{****}p < 0.0001$.

Data availability

All data supporting the findings of this study are included in this published article and its Supplementary Information files. The datasets are also publicly available from the Okayama University Scientific Achievement Repository, ousar.lib.okayama-u.ac.jp. Additional raw data are available from the corresponding author upon reasonable request.

Received: 8 April 2026; Accepted: 7 July 2026
Published online: 15 July 2026

References

1. ICRU Report 46, Photon, Electron, Proton and Neutron Interaction Data for Body Tissues – ICRU. https://www.icru.org/report/photon-electron-proton-and-neutron-interaction-data-for-body-tissues-report-46/.
2. Barth, R. F., Coderre, J. A., Vicente, M. G. H. & Blue, T. E. Boron neutron capture therapy of cancer: Current status and future prospects. *Clin. Cancer Res.* **11**, 3987–4002 (2005).
3. Mentana, A. et al. Mapping neutron biological effectiveness for DNA damage induction as a function of incident energy and depth in a human sized phantom. *Sci. Rep.* **15**, 2209 (2025).

4. Li, X. et al. Measurement of electrons from albedo neutron decay and neutron density in near-Earth space. *Nature* **552**, 382–385 (2017).
5. Ferrarini, M. Exposure risk for workers in an hadrontherapy centre and collective and individual protection measures. *G. Ital. Med. Lav. Ergon.* **42**, 257–261 (2025).
6. Azhgirey, I. L. *et al.* Neutron monitors for high energy accelerators. https://doi.org/10.18429/JACoW-RUPAC2018-TUPSA38 (2018).
7. Icrp. Annals of the ICRP Published on behalf of the International Commission on Radiological Protection. https://doi.org/10.1177/ANIB_37_2-4.
8. Suzuki, M. Boron neutron capture therapy (BNCT): A unique role in radiotherapy with a view to entering the accelerator-based BNCT era. *Int. J. Clin. Oncol.* **25**, 43–50 (2020).
9. Coderre, J. A. & Morris, G. M. The radiation biology of boron neutron capture therapy. *Radiat. Res.* **151**, 1 (1999).
10. Goodhead, D. T. Initial events in the cellular effects of ionizing radiations: Clustered damage in DNA. *Int. J. Radiat. Biol.* **65**, 7–17 (1994).
11. Nikjoo, H., O'Neill, P., Terrissol, M. & Goodhead, D. T. Modelling of radiation-induced DNA damage: The early physical and chemical event. *Int. J. Radiat. Biol.* **66**, 453–457 (1994).
12. Moss, R. L. Critical review, with an optimistic outlook, on Boron Neutron Capture Therapy (BNCT). *Appl. Radiat. Isot.* **88**, 2–11 (2014).
13. Santini, M. T., Rainaldi, G. & Indovina, P. L. Multicellular tumour spheroids in radiation biology. *Int. J. Radiat. Biol.* **75**, 787–799 (1999).
14. Hirschhaeuser, F. et al. Multicellular tumor spheroids: An underestimated tool is catching up again. *J. Biotechnol.* **148**, 3–15 (2010).
15. Antonelli, F. 3D Cell Models in Radiobiology: Improving the Predictive Value of In Vitro Research. *Int. J. Mol. Sci.* **24**, 10620 (2023).
16. Sharma, K., Dey, S., Karmakar, R. & Rengan, A. K. A comprehensive review of 3D cancer models for drug screening and translational research. *Cancer Innov.* **3**, e102 (2023).
17. Aizawa, Y. et al. Development and characterization of a three-dimensional organotypic *in vitro* oral cancer model with four co-cultured cell types, including patient-derived cancer-associated fibroblasts. *Biomedicines* https://doi.org/10.3390/biomedicines12102373 (2024).
18. Charalampopoulou, A. et al. The rise of 3D spheroids in radiobiology for assessing tumour radioresistance. *Acta Oncol.* **65**, 46–58 (2026).
19. Sakurai, Y. & Kobayashi, T. The medical-irradiation characteristics for neutron capture therapy at the Heavy Water Neutron Irradiation Facility of Kyoto University Research Reactor. *Med. Phys.* **29**, 2328–2337 (2002).
20. Kapałczyńska, M. et al. 2D and 3D cell cultures – A comparison of different types of cancer cell cultures. *Arch. Med. Sci.* **14**, 910 (2016).
21. Yamamoto, I. et al. The Early Response After Radiation Therapy on Three-Dimensional Oral Cancer Model Using Patient-Derived Cancer-Associated Fibroblasts. *Int. J. Trans. Med.* **5**, 12 (2025).
22. Fukuda, H. Response of normal tissues to boron neutron capture therapy (BNCT) with10 b-borocaptate sodium (BSH) and 10 b-paraboronophenylalanine (BPA). *Cells* **10**(11), 2883 (2021).
23. Park, H. J., Griffin, R. J., Hui, S., Levitt, S. H. & Song, C. W. Radiation-induced vascular damage in tumors: Implications of vascular damage in ablative hypofractionated radiotherapy (SBRT and SRS). *Radiat. Res.* **177**, 311–327 (2012).
24. Hirose, K., Sato, M., Ichise, K. & Aoki, M. Dose rate effect on cell survival in BNCT. *Curr. Issues Mol. Biol.* **45**, 6986–6994 (2023).
25. Raitanen, J. et al. Comparison of radiation response between 2D and 3D cell culture models of different human cancer cell lines. *Cells* **12**, 360 (2023).
26. Kato, I. et al. Effectiveness of boron neutron capture therapy for recurrent head and neck malignancies. *Appl. Radiat. Isot.* **67**(7–8 Suppl.), S37–S42 (2009).
27. Igawa, K., Izumi, K. & Sakurai, Y. Development of the Follow-Up Human 3D Oral Cancer Model in Cancer Treatment. *Biotech* **12**(2), 35 (2023).
28. Yu, L. S. et al. Tissue architecture influences the biological effectiveness of boron neutron capture therapy in *in vitro/in silico* three-dimensional self-assembly cell models of pancreatic cancers. *Cancers (Basel)* **13**, 4058 (2021).
29. Barcellos-Hoff, M. H., Park, C. & Wright, E. G. Radiation and the microenvironment - tumorigenesis and therapy. *Nat. Rev. Cancer* **5**, 867–875 (2005).
30. Krisnawan, V. E., Stanley, J. A., Schwarz, J. K. & Denardo, D. G. Tumor Microenvironment as a Regulator of Radiation Therapy: New Insights into Stromal-Mediated Radioresistance. *Cancers (Basel).* **12**, 1–25 (2020).

Acknowledgements

We would like to thank all the staff at the Institute of Central Research Laboratory, Okayama University Medical School, for their assistance with the histological analysis and the Institute for Integrated Radiation and Nuclear Science, Kyoto University, for their technical assistance during the irradiation.

Author contributions

K. Igawa conceived the study, S.L. and I.Y. assisted by K.Igawa, K.Izumi and K.S. performed 2D and 3D cell culture experiments. Y.S. and N.K.provided thermal neturon source and performed the dose calculation. K.Igawa performed the neutron irradiation in 2D and 3D cell culture. S.L and I.Y. conducted the violability analysis and S.L. performed the histological analysis. S.L. and K.I wrote the manuscript with input from all authors. All authors discussed the results and commented on the manuscript.

Funding

This work was supported by JSPS KAKENHI Grant Number 23K11918 and 26K15717.

Declarations

Competing interests

The authors declare no competing interests.

Additional information

Supplementary Information The online version contains supplementary material available at https://doi.org/10.1038/s41598-026-61693-2.

Correspondence and requests for materials should be addressed to K.I.

Reprints and permissions information is available at www.nature.com/reprints.

Publisher's note Springer Nature remains neutral with regard to jurisdictional claims in published maps and institutional affiliations.

Open Access This article is licensed under a Creative Commons Attribution-NonCommercial-NoDerivatives 4.0 International License, which permits any non-commercial use, sharing, distribution and reproduction in any medium or format, as long as you give appropriate credit to the original author(s) and the source, provide a link to the Creative Commons licence, and indicate if you modified the licensed material. You do not have permission under this licence to share adapted material derived from this article or parts of it. The images or other third party material in this article are included in the article's Creative Commons licence, unless indicated otherwise in a credit line to the material. If material is not included in the article's Creative Commons licence and your intended use is not permitted by statutory regulation or exceeds the permitted use, you will need to obtain permission directly from the copyright holder. To view a copy of this licence, visit http://creativecommons.org/licenses/by-nc-nd/4.0/.

© The Author(s) 2026